SOFT ROBOTS

Haptiknit: Distributed stiffness knitting for wearable haptics

Cosima du Pasquier[1]†*, Lavender Tessmer[2]†, Ian Scholl[1], Liana Tilton[1], Tian Chen[3], Skylar Tibbits[2], Allison Okamura[1]

Haptic devices typically rely on rigid actuators and bulky power supply systems, limiting wearability. Soft materials improve comfort, but careful distribution of stiffness is required to ground actuation forces and enable load transfer to the skin. We present Haptiknit, an approach in which soft, wearable, knit textiles with embedded pneumatic actuators enable programmable haptic display. By integrating pneumatic actuators within high- and low-stiffness machine-knit layers, each actuator can transmit 40 newtons in force with a bandwidth of 14.5 hertz. We demonstrate the concept with an adjustable sleeve for the forearm coupled to an untethered pneumatic control system that conveys a diverse array of social touch signals. We assessed the sleeve's performance for discriminative and affective touch in a three-part user study and compared our results with those of prior electromagnetically actuated approaches. Haptiknit improves touch localization compared with vibrotactile stimulation and communicates social touch cues with fewer actuators than pneumatic textiles that do not invoke distributed stiffness. The Haptiknit sleeve resulted in similar recognition of social touch gestures compared to a voice-coil array but represented a more portable and comfortable form factor.

INTRODUCTION

The sense of touch is crucial to performing everyday tasks such as walking, cooking, and typing. Without touch feedback, known as haptics, we lose an enormous component of our interaction with the world, in particular with other human beings. Touch is used in common social interactions, including soothing, expressing power, and playing (*1*). Contrary to the belief that touch merely complements speech or vision, it can serve as the sole communication channel for emotions such as anger, fear, love, and gratitude (*2*). Human tactile perception results from the integration of signals from diverse skin mechanoreceptors, each specialized in responding to specific stimuli. For example, Pacinian corpuscles detect high-frequency vibrations, Meissner corpuscles respond to the rate of skin deformation, Merkel discs focus on spatial features, and Ruffini endings are sensitive to skin stretch (*3*, *4*). In addition, hairy skin, like that on the forearm, houses C tactile (CT) afferents activating the insular cortex, a region implicated in emotional processing (*5*, *6*). Wearable haptic devices stimulate these mechanoreceptors to enhance artificial touch interactions, offering the possibility of conveying nuanced and realistic tactile experiences. Haptic devices can provide guidance (*7*), convey abstract information like emotions or mood (*8*), or provide additional inputs in multitasking (*9*). Commercial products like smartphones and smartwatches with haptic feedback primarily rely on vibration feedback from electromagnetic actuators, which meet practical constraints in size, weight, and power. However, vibration feedback is difficult to localize because of the large receptive fields of Pacinian corpuscles and is not able to realistically convey slowly varying touch interactions.

An alternative approach to mobile touch interaction has been emerging, inspired by the field of soft robotics. Pneumatic actuators can produce quasistatic displacement, shear, and compression to communicate information to the wearer (*7*) and are attractive because they can rapidly achieve relatively high forces (*10*, *11*). Soft actuators also have a stiffness profile close to that of skin (*12*), promoting a snug fit and comfort. Wu and Culbertson (*13*) demonstrated that pneumatic actuators outperformed voice-coil motors in continuity and pleasantness, and Shtarbanov *et al.*'s (*14*) pilot study found that pneumatic indentation was more enjoyable than other haptic sensations like suction and voice-coil motors. However, the use of exclusively soft materials comes at a cost: Soft materials do not typically offer strong grounding, which limits the achievable intensity of reaction forces and sensations (*15*). For example, the soft linear pneumatic actuators embedded in the haptic device by Kanjanapas *et al.* (*15*) produce a maximum force of 0.7 N. To address this issue, most pneumatic haptic sleeve designs use large, distributed actuation to produce generalized sensations of compression and stretch (*16*, *17*) but require bulky and rigid hardware for pressure regulation and monitoring.

Recently, a design paradigm has emerged to enable high-intensity haptic stimulation while enabling mobility and comfort: combining soft pneumatic actuators with knit textiles. The modernization of knitting has transformed this millennia-old tradition into a state-of-the-art industrial fabrication method. Knit textiles hold two main advantages that make them attractive in applications driven by human-computer interaction (HCI): Their inherent compliance, which allows them to conform to doubly curved surfaces without compromising their flexibility, and the high-resolution control that flatbed knitting gives the designer over local mechanical properties through localized specification of the material, pattern, and stitch (*18*–*20*). Like soft pneumatic actuators, the capacity of knits to adapt to the wearer's morphology promotes comfort and usability. The potential of knits for HCI was described by Luo *et al.* (*21*), who presented knit sensing interfaces with conductive yarns embedded in wearable garments and modulations in stitch and material to control pneumatic deformation in a manner similar to classic

[1]CHARM Laboratory, Stanford, CA, USA. [2]Self-Assembly Laboratory, Massachusetts Institute of Technology, Cambridge, MA, USA. [3]Architected Intelligent Matter Laboratory, University of Houston, Houston, TX, USA.
*Corresponding author. Email: cosimad@stanford.edu
†These authors contributed equally to this work.

fiber-reinforced elastomeric enclosures (*22*). Kim *et al.* (*23*) first showcased knitting as a source of haptic feedback with KnitDermis, which provides tactile stimulation using shape memory alloy microsprings integrated in knit channels, and later KnitSkin (*24*), a tubular actuated knit robot that can travel up the arm. Sanchez *et al.* (*25*) produced thermally actuating textiles that used phase change to inflate actuators without an external pressure source. However, the full potential of industrial automated knitting for haptic applications remains underdeveloped; there are few examples that leverage embedded material properties and incorporate component assemblies. Existing research used homogeneous knit fabric as an armature and a vehicle (*26*) rather than as a key component of the system.

In this work, we propose to use distributed stiffness knitting to enable perceivable patterned haptic sensations, an approach we call Haptiknit. This concept is embodied in a fully integrated soft pneumatic haptic sleeve with distributed stimulation to the skin of the forearm (Fig. 1). The sleeve is knitted as one piece, composed of two main layers subdivided into six textile sublayers, that achieves stiffness variations of more than two orders of magnitude by controlling its topology and material. Designed and shaped to conform to the forearm, it allows seamless integration of multiple sets of soft actuators through the selective use of heat-fusible yarn. We characterized the force generation, cycling behavior, and frequency response of the three-dimensional (3D)–printed actuators for integration with a Haptiknit sleeve and show that each actuator could achieve forces above 40 N. The sleeve is powered by an unencumbering, untethered pneumatic supply system worn on the upper arm as a self-contained unit. We validated the ability of this sleeve to effectively convey haptic feedback by replicating the actuator configuration of another haptic sleeve that used voice-coil motors (*8*). We benchmarked our device in a three-part human user study that showcased the Haptiknit sleeve's performance for discriminative and affective touch. An overview of the fabrication method and the functioning of Haptiknit can be seen in Movie 1.

RESULTS

Distributed stiffness knitting

To enable high-resolution haptic feedback in our sleeve, we implemented distributed stiffness to control the deformation of soft pneumatic actuators with fabric. As shown in Fig. 1, we embedded actuators between two layers of fabric, one soft and one stiff, to direct deformation against the skin. Computer numerically controlled knitting, the modern form of industrial knitting, enabled us to control stiffness locally through the choice of textile topology (type of knot and type of pattern) and material in one seamless fabric construction (*18*).

We approached stiffness distribution in two ways: by varying the knit topology and by selectively adding a heat-fusing agent in high-stiffness zones during fabrication. First, we demonstrated how modifying only the topology affected stiffness. Figure 2A provides force-displacement curves from uniaxial testing in the course direction for three soft textiles made from the same yarn (Yeoman 540 Denier 80/20 nylon/Lycra) with varying topology. Fabric A was a single-layer ½-gauge rib, fabric B was a double-knit ½-gauge single jersey (front) and ¼-gauge single jersey (back), and fabric C was a three-layer spacer fabric with double-knit single gauge jersey (front and back) and tucks in the midlayer. The differences in topology are visible in the microscope images in Fig. 2A. In these examples, stiffness varied by a factor of 8.43, and the textiles exhibited typical hyperelastic behavior. Sample videos from the uniaxial tests for fabrics A, B, and C are shown in movie S1. Uniaxial testing results of the fabrics in the wale direction are shown in fig. S3A.

Second, we selectively embedded thermoplastic fusible yarn in the knit, which was melted in a heat-setting postprocessing step to produce a global stiffening effect. To create high-stiffness zones with sufficient contrast to fully direct the load transmission of the soft pneumatic actuators, we tested three different amounts of heat-fusible yarn (HMS-Griltech 390 Denier Grilon K85) in the course direction: fabric D at 28.3%, fabric F at 44.4%, and fabric G at 54.2% of the total fabric weight, respectively. We used the same base fabric knit and the same yarn as in the low-stiffness fabrics. Results

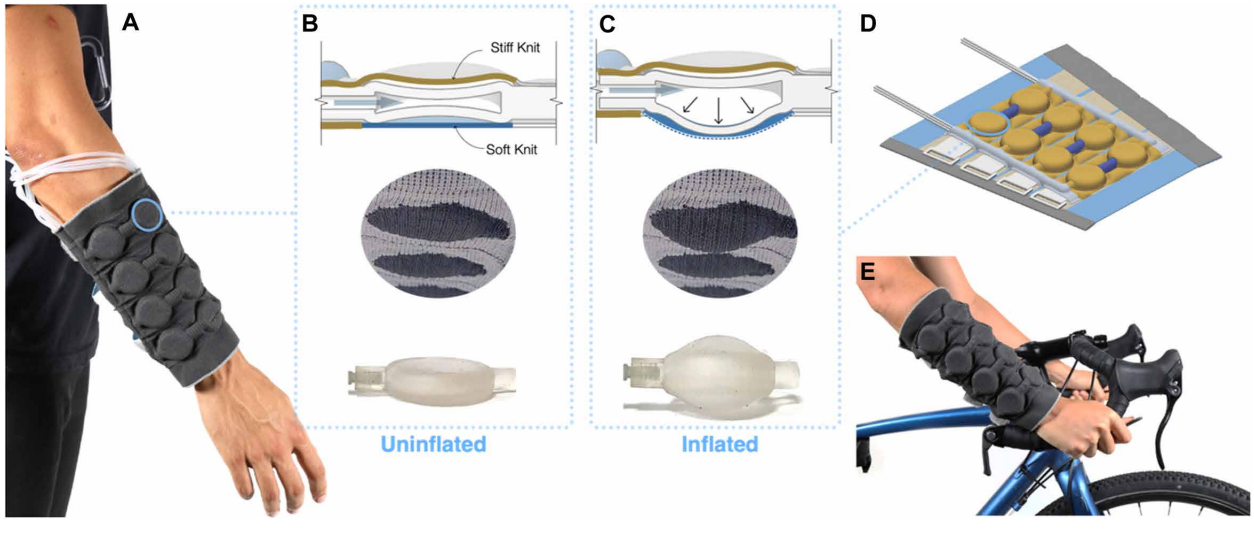

Fig. 1. Haptiknit system overview. (**A**) A Haptiknit-powered sleeve is composed of multiple knit layers of distributed stiffness and embedded pneumatic actuators; with eight actuators and an untethered controller, it provides multimodal haptic signals. The (**B**) uninflated and (**C**) inflated states of the sleeve are shown schematically, in the sleeve, and outside the sleeve. The sleeve is knit in a single piece (**D**) and has applications, for example, in navigation (**E**).

presented in Fig. 2B show that the incremental increase in heat-fusible yarn concentration produced a maximum stiffening factor of 4.9, resulting in an almost 400-fold difference from the softest to the stiffest textile, as indicated by the effective stiffnesses in Fig. 2D. As the amount of heat-fusible fiber doubled and then tripled, more bubbles from hardened resin appeared in the microscopy images (to the right of the graph in Fig. 2B), and the material exhibited increasingly plastic behavior. Because of comfort considerations, we used only fabric D in the sleeve, given that testing showed that its stiffness was sufficient for load transmission. As shown in Fig. 2C, the fabric transitioned from the typical hyperelastic response of a textile to a plastic response before and after heat setting, with a stiffening factor of 19.6. Sample videos from the uniaxial tests for fabrics D, E, and F are shown in movie S2. Uniaxial testing results for the fabrics in the wale direction are shown in fig. S3B.

Movie 1. Overview of design, fabrication, and performance of Haptiknit.

Prototype fabrication and characterization

Our haptic sleeve prototype shown in Figs. 1 and 3 contained three integrated components: the sleeve, the actuators, and the air supply system. Each component was designed and characterized prioritizing comfort, discernability of haptic feedback, and portability.

Wearable knit haptic sleeve

We distinguished haptic feedback zones from inert zones in the knit sleeve by adjusting the textile stiffness through a combination of material and stitch type variations and heat treatment. Low-stiffness regions were knit using elastic yarns (fabrics A, B, and C), whereas high-stiffness regions resulted from heat setting specific areas with thermoplastic fibers (fabric D). The primary design requirement of the knit sleeve was to transfer actuator forces onto the skin for a wide range of arm sizes. The design also had to accommodate the assembly and installation of pneumatic actuators and the routing of tubes. This was achieved with compartments, channels, and a multilayer surface topology. We include a detailed knitting file in the Supplementary Materials.

The knit sleeve is organized into two major layers: an inner layer in contact with the skin and an outer layer within which the actuators are inserted and tubing is routed. These two layers are each composed of three individual sublayers (six sublayers in total). The sublayers each contain specific configurations of high- and low-stiffness regions as shown in Fig. 3. Low-stiffness fabric regions (A, B, and C) have three functions. First, the fabric A regions in contact with the inflatable areas of the actuators (in dark blue in Figs. 2 and 3) expand and contract with pneumatic force. Second, two long fabric B regions on each side of the actuators (in gray in Figs. 2 and 3) allow for easy routing of the hoses from actuators to the air supply system. Third, narrow transverse elastic fabric C regions are situated between each actuator (in light blue in Figs. 2 and 3), allowing the entire system to flex, twist, and adapt to each user's unique body shape. We achieved this by modifying the knit topology only, using the same yarn for all three regions. The arrangement of

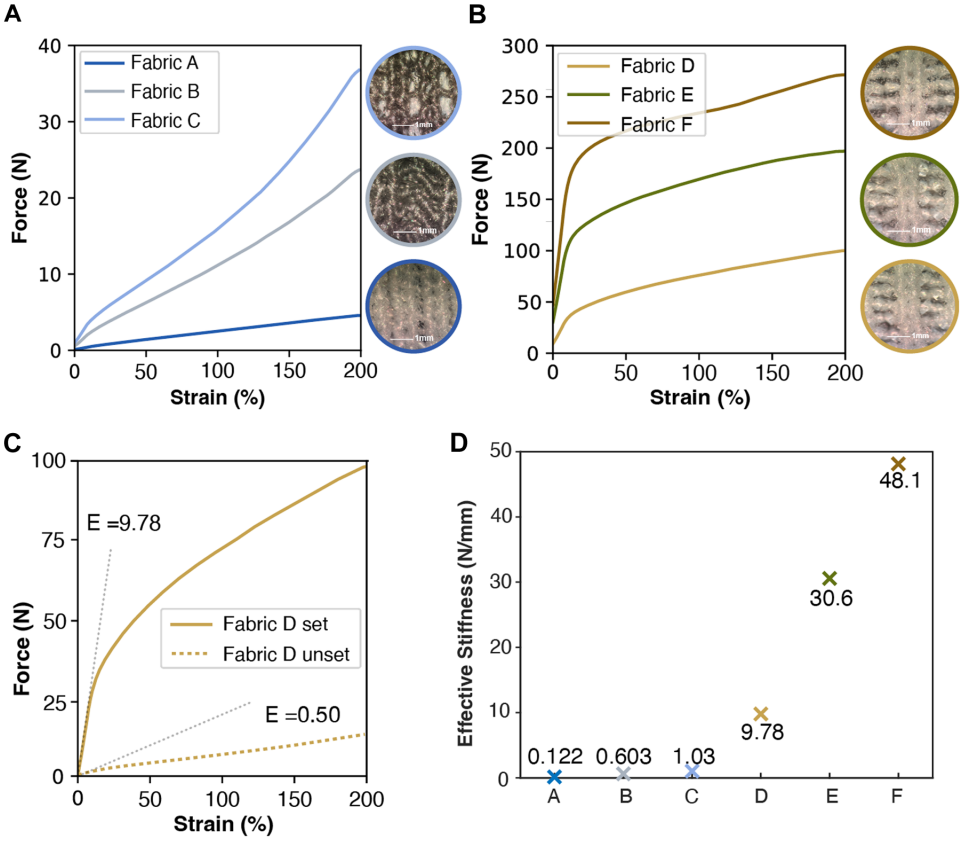

Fig. 2. Stiffness changes using topology variation and bonding fibers. Force-displacement curves in uniaxial testing (course direction) for (**A**) low-stiffness fabrics, where stiffness variation is achieved by changing the topology, and (**B**) high-stiffness fabrics, where stiffness change is achieved by adding thermoplastic fiber. A microscopic view with a magnification of 50 (scale bar in picture) is shown for each fabric. (**C**) Behavior of fabric D before and after heat setting. The effective stiffness *E* is given for both curves, and the linear regression curves used to estimate the effective stiffnesses are marked with a dotted gray line. (**D**) Effective stiffnesses of all materials in N/mm. The stiffest material (fabric G) is 400 times stiffer than the softest material (fabric A).

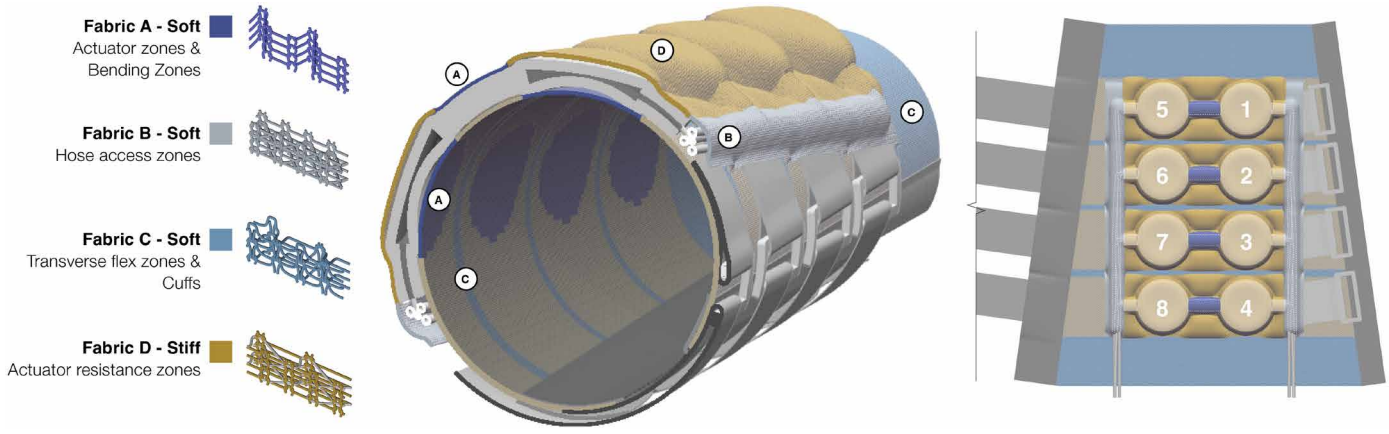

Fig. 3. Haptiknit sleeve construction overview. The 3D view shows the sleeve cross section with circumferential continuity of stiff material integrated with Velcro closures. The materials and knit structures are detailed with consistent color coding throughout the text: Fabrics A, B, and C have the same material and topological variations; fabric D was stiffened using heat-fusible yarn. The 2D view depicts the unrolled sleeve including the locations of the integrated actuators and pneumatic hoses. Although pairs of actuators are connected by a neck for assembly purposes, each actuator is controlled separately.

high-stiffness regions (fabric D) was designed to maintain circumferential continuity of high-stiffness material, which concentrates the actuation forces onto the deformable areas while constraining the assembly against the body. We chose fabric D over fabrics E and F for its balance of target force transmission and user comfort.

The Velcro straps for the sleeve were sized to accommodate the fifth percentile of women's forearm circumference (smallest fit) and the 95th percentile of men's forearm circumference (largest fit) (*27*). One Velcro strap was attached to each actuator region, enabling each of the four actuator pairs to be tightened individually to maintain close skin contact in a wide variety of different arm shapes. The placement of Velcro straps also supported the stiffness continuity around the arm and was easily manipulated by the device wearer during donning and doffing.

Soft 3D-printed actuators

Thanks to 3D printing, we can fabricate custom actuator shapes that can be seamlessly integrated into a textile. We fabricated our soft actuators using an SLA 3D printer (Formlabs Form 3). As shown in Fig. 4C, the actuators had a diameter of 25 mm and were placed on the dorsal side of the forearm in a two-by-four grid, spaced 37 mm apart center to center in the proximal-distal axis and 50 mm in the transverse axis (Fig. 3). These dimensions match those of the sleeve reported by Salvato *et al.* (*8*), allowing us to use their social touch gesture patterns in our user study. Previous research has shown that this layout density effectively communicates continuous motion (*28*) and exceeds the two-point discrimination threshold for the lower dorsal arm (*8*, *29*). A denser array would add complexity without enhancing the haptic experience. The forearm's smooth, consistent curvature and even distribution of mechanoreceptors make it ideal for delivering uniform haptic feedback. Each actuator is individually addressable.

We determined the best material type and actuator thickness by characterizing force responses under two conditions: blocked force of a single actuator as a standalone or between two layers of fabric (one soft, fabric B; and one stiff, fabric D; as shown in fig. S5, A and B) to differentiate the actuators' performances in free space and embedded in a distributed stiffness textile. We chose to investigate force because displacement depends on the user's skin elasticity and thus would vary across users. We tested two materials from Formlabs, Elastic 50A and Flexible 80A, and three wall thicknesses, 1.0, 1.5, and 2.0 mm, a total of six variations. The force testing procedure is detailed in Materials and Methods. We show the mean results in Fig. 4D.

The results in Fig. 4D indicate that all actuator variations achieved at least 35 N at the maximum pressure of 230 kPa. This is more than triple the values obtained by recent work by Jumet *et al.* (*7*) that also used 25-mm-diameter soft pneumatic actuators in a textile sleeve. In the cases where the force is constrained by the stiff and soft textile layers (dashed lines in Fig. 4D), the forces achieved were equal to or very similar to those in the unconstrained tests. The higher forces observed in the constrained tests are due to the fabric between the actuator and sensor, which increased the contact area, in particular at lower pressures. This is illustrated with finite element analysis of the 2-mm Elastic 50A and Flexible 50A actuators in fig. S4.

The higher elasticity of Elastic 50A actuators increases their deformation potential. This directly increases the contact surface with the force sensor, leading to consistently higher values. Thinner actuators achieved greater forces for a similar reason. However, Elastic 50A actuators of 1.5 mm and below had a failure rate of 25%, and 1-mm-thick Flexible 80A actuators had a failure rate of 50%. We chose the pressure to limit force transmission at values under 30 N for comfort and safety concerns. To prioritize system robustness and durability, we used actuators printed with Elastic 50A and a 2-mm wall thickness, achieving maximum forces of 24 N at the standard system pressure (175 kPa). We conducted cyclical tests up to 100 cycles on the final actuator configuration for both setups to ensure consistent performance over time, avoiding issues like material fatigue or hysteresis. As shown in Fig. 4E, the actuators maintained consistent performance. The fabric notably affected force transmission at high (200 kPa) and low (150 kPa) pressures, with slight deformation at high pressure and dampened deformation at low pressure. At the standard pressure (175 kPa), actuator performance remained stable.

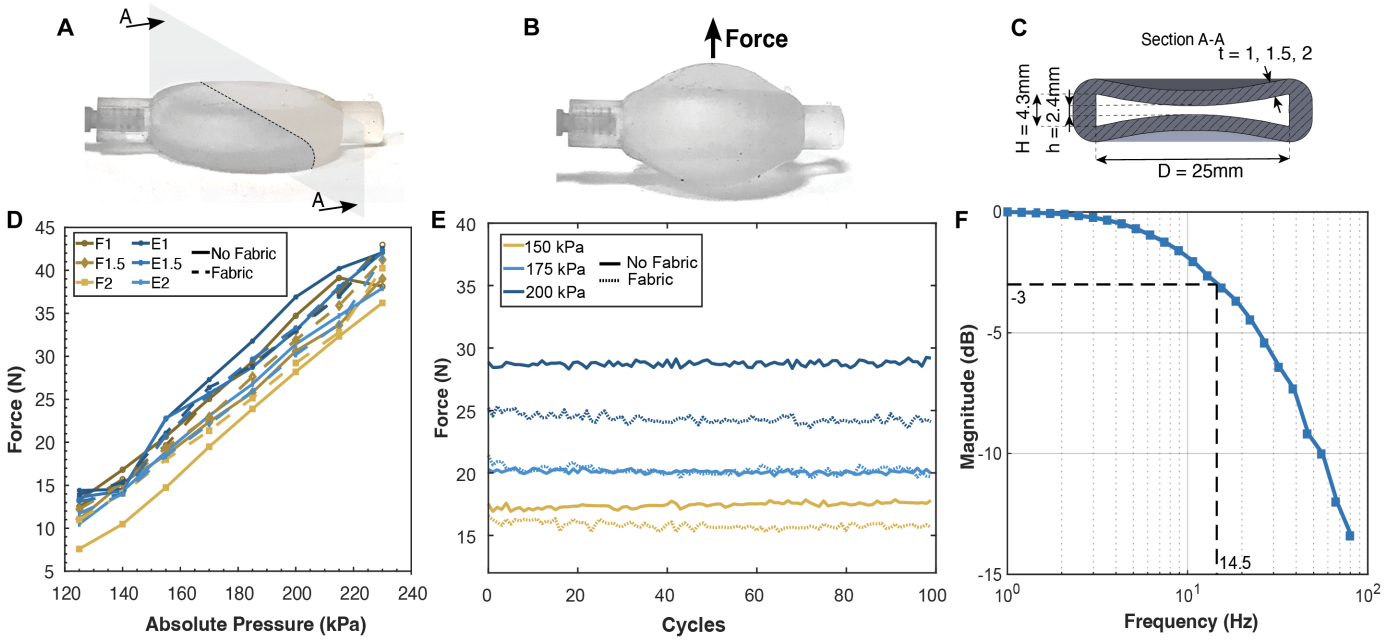

Fig. 4. Soft pneumatic actuator geometry and characterization results. (**A**) Uninflated actuator with section view at the dotted line. (**B**) Inflated actuator as used to measure blocked force between the rest state and the inflated state. (**C**) Section view of uninflated actuator as indicated in (A), including dimensions. (**D**) Blocked force versus pressure for $N = 4$ actuators. F indicates Flexible 80A, and E indicates Elastic 50A, followed by the thickness in mm. Dashed lines indicate that the actuators were tested between a stiff and a soft fabric layer; full lines indicate that they were tested in blocked force with an acrylic plate. (**E**) Force cycling behavior of the final actuator (Elastic 50A, 2 mm), $N = 3$. (**F**) Actuator frequency response magnitude in force; the bandwidth (−3 dB magnitude) is marked with black dashed lines, $N = 3$; averages and SDs are in tables S3 and S4.

We characterized the frequency response and bandwidth of the final actuator configuration (Fig. 5). The −3 dB line in Fig. 4F indicates a reduction of the signal power by 50%, and so the bandwidth, and is reached at frequencies of 14.5 Hz. This means that forces perceived as skin indentation can be varied at frequencies higher than the human volitional movement bandwidth (~10 Hz), which implies that the actuators can induce haptic sensations that feel natural.

Portable pneumatic system for soft haptics

Portability is crucial for the ambulatory potential of wearable devices and so was a priority in our work. To make the development of untethered soft robots more accessible, Shtarbanov (*30*) recently introduced FlowIO, an open-source miniature pneumatic supply system. We developed a customized version of their setup, called AirPort 1.0, to power the actuators, with modifications to address our specific needs (see details in Materials and Methods).

The final system, shown in fig. S1, weighs 440 g and provides a bistable air supply, where each port can switch independently between the inflation channel supplied by the positive pressure pump and the deflation channel connected to the vacuum pump. Thus, there are four possible states for each port: inflating, holding pressure, deflating with vacuum, and ambient pressure.

AirPort 1.0 compares favorably to other portable pneumatic systems. Programmable Air, the system introduced by Shrivastava (*31*), has a similar form factor but only three output ports and half the pressure range. Although AirPort has a pressure range five times smaller than that of Kim *et al.*'s device (*32*), it offers eight ports instead of one, can pull vacuum, and is six times lighter. It can be comfortably worn around the upper arm for prolonged periods of time using a strap.

User study

We performed a three-part user study with 32 participants to test the sleeve in three scenarios for both affective and discriminative touch (*33*). The tests parallel those performed using previous haptic sleeves using voice-coil motors and/or vibration motors (*28*). The study consisted of a maximum pressure calibration step, three tests, and a postexperiment assessment. In calibration, we determined the maximum pressure based on each participant's preference. In the first test, participants estimated the location of individual actuators (discriminative touch). In the second test, participants experienced and rated nine stroking patterns (affective touch). In the third test, participants interpreted and rated six social touch gestures provided by the sleeve (affective touch). The postexperiment assessment included an open-ended discussion, during which participants provided five ratings on perceived task accuracy and sleeve design. Details of the calibration and testing procedure are given in Materials and Methods.

Individual actuator localization

We evaluated actuator localization accuracy to assess the feasibility of our approach, as opposed to vibration, for creating a tactile display on the forearm. We inflated each actuator to the calibrated maximum pressure three times in random order and asked the participants to guess which actuator had been inflated, using the 1 to 8 location numbering shown in Figs. 3 and 5.

Figure 5 shows the localization performance distribution by actuator. We summed the guesses across all participants and runs for when a specific actuator was inflated. The overall accuracy across the experiment was 69%, more than 5.5 times chance. In every instance, the correct actuator was consistently the top choice, and the

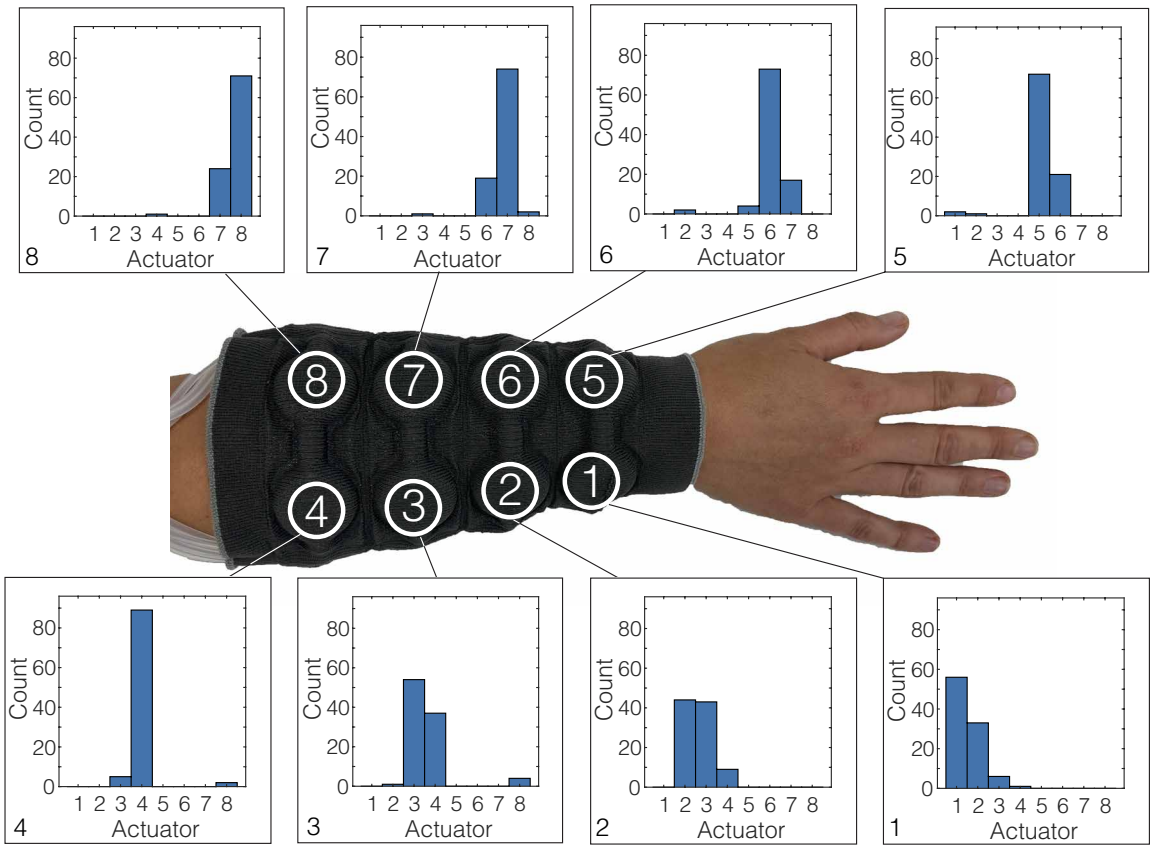

Fig. 5. Actuator localization accuracy results. Localization results for $N = 32$ participants for each of the eight actuator locations; the graph counts indicate how many times the location was chosen across all participants and runs; each actuator location was played three times in a randomized order.

second highest scoring actuator location was directly adjacent and in the same row. The side of the forearm, inner (#5 to 8) or outer (#1 to 4) forearm, was correctly guessed in 98% of the cases. In addition, we observed that the actuation stimuli on the inner side of the forearm were predicted correctly in 76% of the cases, compared with 63% on the outer side of the forearm.

Perception of stroking patterns

To replicate a stroking sensation, we inflated actuators 5 through 8 (as shown in Fig. 5) in sequential order, varying the duration of and delay between each actuation. Delays were defined as the percentage of the inflation duration after which the next actuator in the stroke started to inflate. After each of nine stroking patterns was played, participants were asked to rate their perceived continuity using an 8-point Likert scale, where 0 = discrete and 7 = continuous, and pleasantness using a 15-point Likert scale, where −7 = very unpleasant, 0 = neutral, and +7 = very pleasant.

Figure 6A shows the average continuity ratings normalized to the same 1-to-7 scale used by Culbertson *et al.* (*4*) and their SDs sorted by duration and delay. Rated continuity decreased with inflation duration when delay was held constant and decreased with delay when the duration was held constant.

Similarly, Fig. 6B shows the average pleasantness ratings and their SDs organized by pulse width and delay. All ratings were greater than or equal to zero on average, implying that no stroke was consistently perceived as unpleasant. The pattern with the shortest inflation duration and largest delay was perceived as the most pleasant, whereas increasing the duration generally lowered the pleasantness. For short inflation durations of 200 ms, increasing the delay raised pleasantness; for longer inflation durations, it showed the opposite effect and decreased pleasantness.

Recognition and perception of social touch gestures

Our third and final test measured user recognition of six common social touch "gestures" that were previously studied and mapped to the two-by-four actuator layout by Salvato *et al.* (*8*): attention, gratitude, happiness, calming, love, and sadness. Previous studies showed that these emotions can be signaled through nonverbal communication (*2*, *34*, *35*).

The confusion matrix shown in Fig. 6C displays the aggregated top choices across all participants and runs for each executed gesture, normalized row-wise. Whenever the percentages provided by the participant created a tie for top choice, the point for the top choice was distributed proportionally among the gestures that shared the highest attributed percentage. The total classification accuracy was 36%, 2.2 times the rate of chance. Attention and happiness gestures were guessed correctly at more than three times the rate of chance, with the primary confusion being between these two. Gratitude and sadness were guessed correctly at more than 1.6 times the rate of chance and were also the top choice for their respective scenario. The calming and love gestures exhibited higher levels of confusion, approaching chance levels. This confusion led to participant selection of alternative gestures, with attention replacing calming and gratitude taking the place of love as the top choices, respectively.

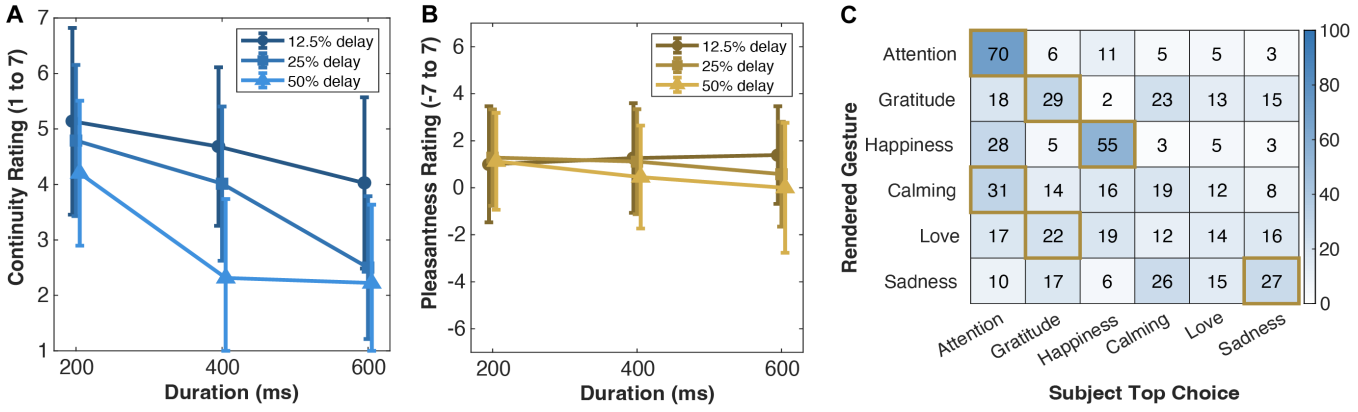

Fig. 6. Stroking ratings and social touch gesture top choice results. (**A**) Continuity and (**B**) pleasantness ratings for three stroke durations and three delays. (**C**) Normalized gesture top choice results for the six emotions communicated with the sleeve. Highest values for participant top choice for each rendered gesture are outlined in gold, the scale on the right represents how many participants guessed correctly (in %), and the bars show the SDs from the mean participant response; $N = 32$.

The recall for a played gesture is the true positive rate, defined as the percentage of how often a gesture was correctly guessed when presented. All of our gestures had recall values 9 to 16% lower than those in the confusion matrix presented in Fig. 6 of Salvato *et al.* (*8*), except for happiness (55% recall in ours compared with 45%). A row-wise Bhattacharyya coefficient calculation (*36*) between our results and theirs, serving as an indicator of the overlap between two distributions, revealed high similarities of 96, 89, 96, 95, 92, and 97% by row and gesture, respectively.

We also asked participants to rate the perceived valence, arousal, and authenticity of each gesture on Likert scales from 1 to 9. Happiness received the highest average valence rating of 6.25 and sadness the lowest, 4.66. Happiness also had the highest average arousal rating of 7.31, more than 1.5 points greater than any of the other rendered gestures. Gratitude had the highest average authenticity rating of 6.88 and happiness had the lowest, 3.41.

Postexperiment ratings

After the experiments, participants were asked to self-assess their performance in the localization and gesture recognition tests. Participants were also asked to rate the ease of donning, comfort, and aesthetics of the Haptiknit sleeve on a Likert scale from 0 = very bad to 10 = very good.

Participants' self-assessment, normalized to a 10-point scale, matched their actual accuracy for both the localization task and gesture task (Fig. 7A). The gesture task had lower accuracy, with a median normalized rating of 4.4 compared with 6.9 of the localization task.

In the postexperiment discussion, participants described the importance of actuation frequency when assessing social touch. Participant 17 (P17) said the following: "Sadness and gratitude I thought of as a slower movement. Attention and happiness was a faster movement. But the nuances between those were more difficult. Love was less defined for me." Applied force was also mentioned as a determining factor by P31: "The lighter [patterns] felt like gratitude or attention. The deeper and more intense [patterns] felt like love, calming, or sadness." Another factor was the location of actuation on the arm, as noted by P31: "Some of the gestures were on one side of the arm and some were on both sides. The ones that were on both sides I interpreted as more intimate or more intense."

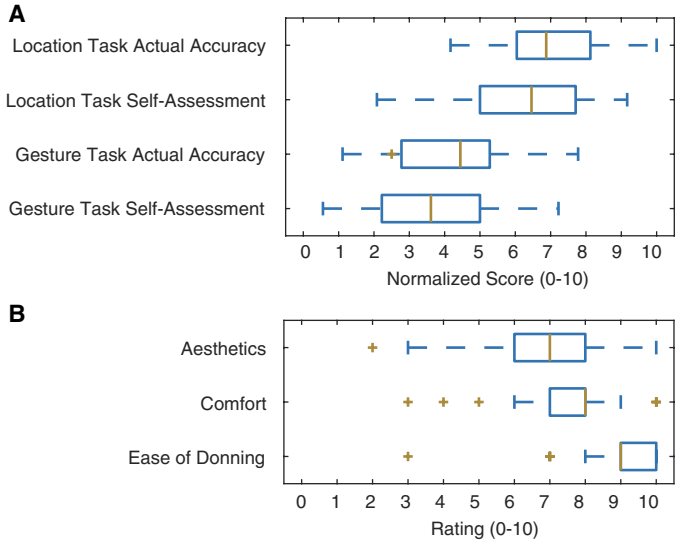

Fig. 7. User study postexperiment ratings. Postexperiment ratings of (**A**) location and gesture task accuracy (self-assessed and measured) and (**B**) self-assessed qualitative description of the sleeve; the data are expressed as a whisker-plot diagram: The box represents the interquartile ranges, whereas the means are indicated by yellow lines; the dashed lines extend out to the lower and upper quartiles; outliers are indicated with yellow crosses.

The results from the Likert scale in Fig. 7B indicated median values of 9 for ease of donning, 8 for comfort, and 7 for aesthetics. Only the aesthetics rating showed mean variations of more than one point in relation with participants' previous experience using human-machine interactive devices. The median aesthetic ratings varied from 6 for individuals with no experience to 7 for those with limited or moderate experience and further increased to 8.5 for individuals with extensive experience. Participant feedback confirmed that key design features, such as selected low-stiffness regions and the closing mechanism of the sleeve, enable easy donning, comfortable wear, and pleasant aesthetics, especially among participants with previous experience testing haptic devices.

DISCUSSION

Distributed stiffness

In our examination of distributed stiffness, we demonstrated the stiffness range attainable through topology variation and material variation (via inclusion of thermoplastic yarn). The stiffness range observed for our soft materials (0.122 to 1.03 N/mm) was comparable to that reported by Singal *et al.* (*37*) (0.003 to 0.223 N/mm). The order-of-magnitude difference can be attributed to the use of only one knit layer in their fabric samples rather than two in fabrics B and C (see table S2). On the other hand, the stiffness range observed for our stiffer materials (9.78 to 48.1 N/mm) was two orders of magnitude higher than those for our and Singal *et al.*'s stiffest unreinforced fabrics.

In our actuator characterization, we showed that constraining the pneumatic actuators with fabric B (effective stiffness 0.603 N/mm) had only a negligible effect on load transmission and deformation, whereas fabric D (effective stiffness 9.78 N/mm) essentially caused a "blocked force" response in that direction. We conclude that to control and direct the load transmission of our actuators effectively, we need a stiffness asymmetry of roughly one order of magnitude. A single, homogeneous fabric could not simultaneously provide haptic feedback accurately and anchor the actuators effectively. An equally important consideration is that the inclusion of the heat-fusible yarn essentially transforms the fabric stretch response from that of tangled yarn to a monolithic material. Consequently, the fabric retains the ability to bend and conform comfortably to the arm, but does not stretch, and effectively blocks any deformation caused by the actuators.

Although one could replicate our distributed stiffness method by assembling, for example, a polymer and a fabric with the appropriate stiffnesses, the design and fabrication processes would be challenging, especially for a wearable device. In contrast, our multilayer knit can deliver the required level of asymmetric response through one-shot manufacturing and a single post-processing step, considerably simplifying the entire procedure. It also allows for building further complexity into a design without scaling the fabrication effort, which opens possibilities to adapt the design to other more complex body parts (joints for example) or entirely different applications.

Haptiknit sleeve prototype

The implementation of the haptic sleeve in our user studies supports the viability of using soft pneumatic actuators and distributed stiffness knitting in wearable haptic devices for both affective and discriminative touch. Although haptic sensations might differ from those caused by vibration or voice-coil motors, we have shown that they are equally or more pleasant, can provide the feeling of continuous motion, and are more successful in communicating granular information. This motivates other applications requiring detailed haptic feedback, such as teleoperation (Fig. 8A), sensory remapping (Fig. 8B), navigation (Fig. 8C), or training movement or communication between players on a team (Fig. 8D).

In addition to providing haptic stimuli, other features of the sleeve and Airport 1.0 are noteworthy. Our pneumatic supply system controls eight individual actuators and a force transmission range of 40 N; this is distinguished from the prior work shown in table S1. Whereas other user studies have used pneumatic supply systems that require additional packaging on the back or the waist, our system is battery powered and untethered and can be worn on the arm alone. Participant feedback in the postexperiment discussion confirmed that combining distributed stiffness knitting with soft actuators and Velcro straps was comfortable and easy to use. In contrast with previous haptic sleeves, our device can thus be worn for prolonged periods of time without affecting the participant's dexterity or mobility. In contrast, the voice-coil system of Salvato *et al.* (*8*) was heavier and prone to overheating because of quasi-static driving of the electromagnetic actuators, thus requiring longer rest periods during user testing. These results demonstrate the potential of combining distributed stiffness knits with soft pneumatic actuators, opening avenues for HCI applications requiring distributed haptic feedback with comfort and portability.

User study

In this section, we first discuss the results from each part of the user study individually. Then, we discuss the implications of our approach in the wider context of wearable haptic devices.

Localization

Untrained participants were able to predict actuation location with a mean of 69% accuracy compared with a chance value of 12.5% (one in eight actuactors). This indicates that the layout of the actuator grid in our sleeve allows participants to discern haptic information

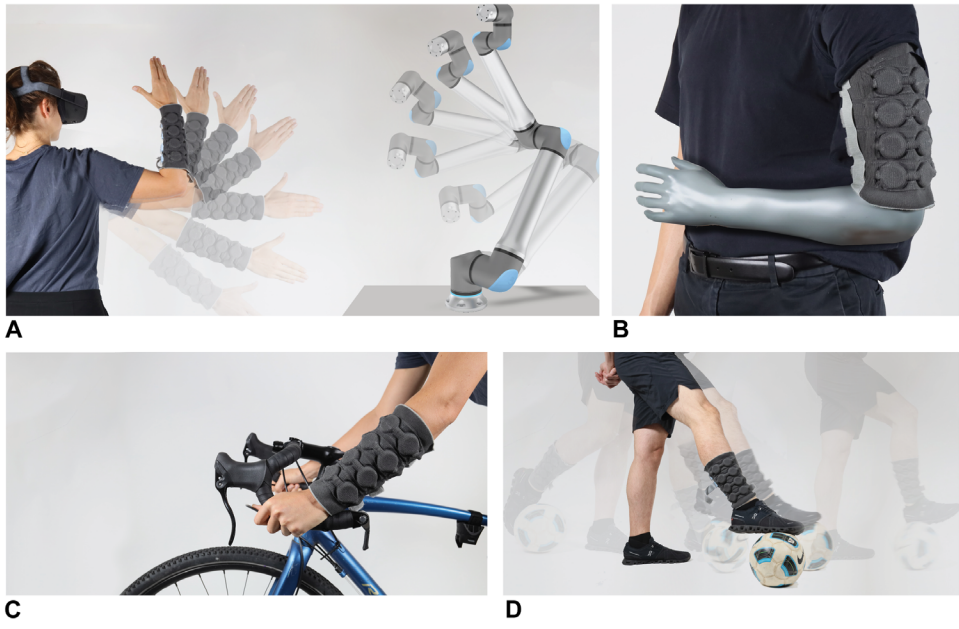

Fig. 8. Potential applications for distributed stiffness haptics. (**A**) Realistic feedback in mixed reality and during teleoperation. (**B**) Sensory remapping, for example, for an instrumented prosthetic arm. (**C**) Navigation, for example, to provide direction guidance that does not obstruct users from seeing and hearing their environment. (**D**) Guidance and communication during sports.

accurately. We believe the selected sparseness of the actuators was a good compromise between making them distinguishable and enabling a continuous stroke as described above. Compared with Jumet *et al.* (*7*), who also demonstrated a pneumatic textile sleeve, we achieved communication of eight cues with eight actuators, outperforming their method that conveyed only four cues with 12 actuators.

The radial nerve wraps around the elbow and then lies on the inner forearm until reaching the index finger and thumb. This results in higher sensitivity on the inner than the outer forearm (*38*). Correspondingly, our actuators 5 to 8, which are placed on the inner arm, achieve higher average accuracy values. Our results also align with prior work suggesting that haptic actuation in proximity to body landmarks (also known as anchor points), like the elbow and actuator 4 in our setup, is more easily distinguishable (*28*, *39*). Even for actuators with lower accuracy values (actuators 2 and 3 for example), actuator locations were only confused with their direct neighbors. In similar actuator localization studies that used vibration stimuli, participants typically achieved accuracy ranging from 35 to 55% on the forearm (*28*). In contrast, our study reports a higher accuracy range of 44 to 89%. Vibrotactile actuators stimulate the Pacinian corpuscles, which have large receptive fields, and create vibration waves that propagate through the skin (*39*, *40*), causing a larger area of mechanoreceptors to be activated; these characteristics make vibration actuator locations harder to discern. We conclude that our quasistatic displacement-based haptic approach is more successful for discriminative touch and thus better suited for applications such as a haptic display for communication.

Stroking patterns

Previous literature indicates that stroking motions between 1 and 10 cm/s are most pleasant, because of the response of CT afferents (*6*). However, our slowest stroking pattern, which falls within this speed range (600 ms and 50% delay is equivalent to 7.4 cm/s), was rated lower by more than 1.25 points in pleasantness compared with the highest rated stroke at 13.5 cm/s (200 ms and 50% delay), as shown in Fig 6. Our highest speed stroke at 40.3 cm/s for 200 ms and 12.5% delay also received a continuity rating almost three points higher than that for the slowest one. This is likely due to the discrete nature of our actuation, both spatially and in intensity. Spatially, our stroke is a series of individual contacts, not a continuous stroke as in CT afferent studies (*6*). For intensity, our pneumatic system is open-loop and targets single pressure values; an actuator can only be on or off, albeit at different intensities (stroke depths) and for different periods of time. We found that stroking patterns of longer duration and delays create a crawling, rather than stroking, sensation along the forearm, where each indentation is easily distinguishable. This could indicate that displacement, in contrast with vibrations, does not activate CT afferents. It is also possible that vibrations generally feel more continuous because they excite a larger portion of the skin around the actuator rather than localized deformation.

Despite this observed difference, no stroking pattern was consistently rated as unpleasant. In contrast, Culbertson *et al.* (*4*) reported negative pleasantness ratings for a similar device using voice-coil actuators for strokes of 200 ms and delays of 12.5% or 50%. We attribute the higher pleasantness of our device to the elasticity and comfort of the knit sleeve and soft actuators, in contrast with the rigid and perhaps more robotic feel of voice-coil actuators. We also observed that the sleeve's actuator grid is dense enough to create stroking sensations with middling continuity ratings, as shown in Fig. 6A. The shortest inflation duration of 200 ms and delay of 12.5% received a continuity rating greater than 5 on the 7-point Likert scale.

Social touch gestures

The confusion matrix obtained for the six touch gestures is similar to that in Salvato *et al.*, whose actuator grid dimensions and gesture patterns we replicated (*8*): All Bhattacharyya similarity coefficients for both studies were higher than 89%. However, we achieved an overall lower accuracy: 36% compared with 45%. We believe that this is again due to the nature of our pneumatic control system. In Salvato *et al.*, each actuator stroke could be controlled independently to a specific indentation force. Our current control system only defines whether one or multiple actuators are on or off and the pressure they initially inflate to.

Despite differences in actuation approach, our social touch identification results generally align with those of Salvato *et al.*: Our sleeve can successfully communicate human emotions, as shown in the recall of attention and happiness. These two gestures entailed distinguishable fast actuation patterns, such as a double tap for attention or a series of short and sharp indentations across the forearm for happiness. Arousal and valence also play a role in how effectively an emotion was communicated. Happiness, a high-accuracy gesture, achieved the highest scores, whereas sadness, a low-accuracy gesture, achieved the lowest. In addition, the gestures for calming and love were characterized by more complex and slow actuation patterns, including stroking or squeezing, and test participants reported they were generally less well defined even when given their meaning. As previously observed by Bann and Bryson (*41*), cultural background and age might also affect how these specific emotions are communicated and understood. Our haptic sleeve might be better suited to transmit well-defined and widely accepted social touch gestures. Gratitude, for example, was rated as the most realistic. It consisted of a single squeeze on the lower forearm, like that of a hand.

Conclusion

Our study demonstrates the potential of combining distributed stiffness knits with soft pneumatic actuators, offering an original approach for designing wearable haptic devices with enhanced comfort and portability. The multilayer knits enable effective control over load transmission and deformation in pneumatic actuators, simplifying the design and fabrication processes compared with alternative methods.

The Haptiknit sleeve prototype supports the feasibility of using soft pneumatic actuators and distributed stiffness knitting for affective and discriminative touch in wearable haptic devices. The positive participant feedback on comfort and ease of use underscores the practicality of the proposed approach for long-term wear. The prototype also distinguishes itself by incorporating an untethered pneumatic system with individual actuator control, a wide force transmission range, and the ability to be worn for prolonged periods without hindering dexterity or mobility. Although the user study revealed discrepancies in user preferences for stroking patterns compared with existing literature, the overall pleasantness of haptic sensations, coupled with successful actuator localization and social-touch gesture communication, supports the efficacy of our approach.

Our research introduces an innovative framework for the design and implementation of wearable haptic devices, paving the way for enhanced HCI applications. The combination of distributed

stiffness knits and soft pneumatic actuators offers a promising avenue for the development of comfortable, portable, and versatile haptic interfaces with diverse applications in the fields of communication, interaction, and beyond.

MATERIALS AND METHODS

Distributed stiffness fabric characterization

Homogeneous swatches were knitted using the specifications listed in table S2. Each refers to a specific region of the sleeve prototype. We began by obtaining optical microscopy images (Nikon Eclipse MA200) with a magnification of 50 from these textile swatches before mechanical testing.

We then adapted the ASTM D4694-96 Standard (*42*) to characterize the tensile properties of the different fabrics. We used a universal testing machine (Instron 68SC-2) with tensile grips to apply tension. To prepare the samples, we laser cut rectangular patches of size 80 mm by 40 mm using a carbon dioxide (CO_2) laser engraver (Trotec Speedy 360) from each textile swatch. Three patches were cut in each course direction as indicated by the orientation of the longer edge. From these, we clamped both the top and the bottom edges with polymethyl methacrylate clamps as shown in fig. S2 so that the gauge area was 40 mm by 40 mm. Considering that some yarns are viscoelastic, we ensured a constant displacement rate of 1 mm/s. Maximum strain was set to 200%. We captured the deformation with a digital video camera to further understand the damage mechanisms. We calculated the effective stiffness of the fabrics by fitting a line of best fit to 5% strain using the following equation

$$E = \frac{\sum x_i y_i}{x_i^2} \tag{1}$$

where x_i is the strain in % and y_i is the force in N.

AirPort 1.0 specifications

AirPort 1.0 was adapted from the open-source design known as FlowIO by Shtarbanov *et al.* (*30*). First, we increased the number of output valves from five to eight to control each actuator in the sleeve independently. Second, we also changed the pumps and used the Skoocom SC3802PM positive pressure pump from FlowIO's large-sized pump module and a Skoocom SC1804PM vacuum pump from the medium-sized module to obtain the pressure range needed for the soft pneumatic actuators. Third, we removed the block on the second common air channel of FlowIO's SMC S070 solenoid valves.

Actuator characterization test setup

Force was measured with a Nano 17 sensor (from ATI Industrial Automation). We characterized actuators using two soft materials (Elastic 50A and Flexible 80A resins from Formlabs, where 50A and 80A are the shore hardness) and three bellow thicknesses (1.0, 1.5, and 2.0 mm). The force test setups are shown in fig. S5 (A and B). Each parameter combination was tested $N = 4$ times using new actuators each time. See table S3 for means and SDs.

The cycling behavior of actuators was tested for the final actuator configuration (Elastic 50A at a 2-mm thickness) using the same test setup as above (fig. S5, A and B). $N = 3$ actuators were tested at three pressures (150, 175, and 200 kPa) each and for each test setup (total of nine actuators per setup). In one cycle, pressure was ramped up to the target value and held for 1 s, then the actuator was deflated to atmospheric pressure and held again for 1 s. Actuators were tested for 100 cycles. See table S3 for means and SDs.

The frequency response and bandwidth were measured $N = 3$ times in the unconstrained setups (no fabric, as shown in Fig. 2A) using a square-wave pneumatic input at the nominal system pressure of 185 kPa. We induced a frequency sweep starting at 1 Hz with increments of a factor of 1.2. We measured the force response F, computing each magnitude in dB $20 \cdot \frac{F}{F_{\max}}$. Forces were measured up to 80 Hz, nearing the solenoid valves' switching delay limit (see fig. S6 for time versus pressure response). The frequency-dependent force response is influenced by hardware like pumps and valves. Prioritizing wearability over high-frequency performance, we tested the system's limits and opted not to use larger components.

Design and fabrication of the knit sleeve

The sleeve was designed in the Create+ software interface and fabricated on a STOLL CMS 330 HP-W TT Sport industrial flatbed knitting machine. All knitting layers were fabricated simultaneously in a single seamless textile. As shown in the assembly process in fig. S7, when heat was applied in postprocessing, the layers bonded and stiffened.

The sleeve assembly began by placing four pairs of soft actuators inside designated compartments within the sleeve. Once positioned, the entire sleeve was placed in an oven and heated to 115.5°C for 10 min. After heating, a die shaped to match the dimensions and positioning of the actuators was pressed down on the compartments for 45 s to secure the actuators in place. The sleeve was then placed onto a conical tube, shaped roughly like a forearm, to form its structure. After cooling, Velcro straps were attached at the level of the actuator compartments, ensuring a snug fit to the skin and enabling easy donning and removal of the sleeve (see fig. S7 for a visual guide to the steps).

User study design

Participants were recruited via university email lists, with a focus on ensuring a diverse range of responses across age and gender. Participants provided informed consent, and the protocol received approval from the Stanford University Institutional Review Board. Thirty-two participants (18 males, 13 females, and 1 who preferred not to answer; ages 18 to 58 years) took part in the study. Twenty-five participants reported that they were right-handed, six left-handed, and one ambidextrous. Ten of the participants had extensive prior experience with haptic devices, 5 moderate, 10 limited, and 7 had no experience. None of the participants reported cognitive or sensory impairments. The ethnicity information of the participants was not collected at the time of the study.

Participants wore the sleeve on their right forearm with the actuators located on the dorsal side. During the experiment, participants rested on their elbow with the forearm and sleeve held freely in the air, hidden by a box as shown in fig. S8. They wore active noise-canceling headphones playing white noise. The modes of actuation were controlled by the experimenter on a custom graphical user interface (fig. S8).

We calibrated the sleeve output for each participant. During calibration, we determined the first pressure at which participants could feel the indentation from actuators and the pressure at which the indentation started to feel uncomfortable. We activated a single actuator (#7) starting from 115 kPa and increased the pressure in

increments of +15 kPa until the participant indicated they could feel the actuator by saying "yes." We continued ramping up the pressure in similar increments until participants indicated the pressure started to feel uncomfortable, upon which calibration was stopped. This procedure was repeated twice for each participant. The average minimum system-controllable indentation felt by participants was 115 kPa, and one participant felt discomfort at 166 kPa (others felt no discomfort). The maximum pressure in the experiment was then set to the maximum comfortable pressure for each participant.

Stroking continuity

We used durations of 200, 400, and 600 ms and delays of 12.5, 25, and 50%, a subset of the modes Culbertson *et al.* (*4*) previously investigated. These nine actuation conditions were repeated twice in a randomized order.

Actuator localization

We inflated actuators to the calibrated maximum pressure one at a time, holding this state for 750 ms and deflating using a vacuum for 500 ms. We then asked the participants to guess which actuator had been inflated, using the 1 to 8 location numbering shown in Figs. 2 and 6. Actuator numbering was provided separately on a printed diagram. Before data collection, the participants were played each actuator once in order of numbering to allow them to develop a frame of reference. For the experiment, each actuator was played three times in a randomized order, resulting in a total of 24 actuation stimuli.

Social touch gestures

For the social touch gesture study, we followed the same protocol as Salvato *et al.* (*8*) to ensure a fair comparison. First, participants listened to six audio prompts describing the social touch scenarios. Next, they experienced each of the six actuator-mapped gestures once in a consistent randomized order for each participant, without any knowledge of the gestures' meaning.

During the experiment, participants were played each gesture pattern three times in a randomized order, adding up to a total of 18 actuation sequences. After each gesture, participants verbally assigned a probability that a specific gesture had been played. They were told to give ratings in percentages from 0 to 100 in 10% increments and that their ratings for a single played gesture did not have to sum to 100%.

Last, participants were played each mapped gesture once and were asked for four ratings: valence, arousal, pleasantness, and authenticity (whether the gesture felt like human touch). Valence and arousal scales were rated using printed Self-Assessment Manikins (*43*) with a Likert scale from 1 to 9. Authenticity of the gestures was rated using a printed Likert scale ranging from 0 = very unrealistic to 10 = very realistic.

Statistical analysis

Fabric characterization

For each fabric, we tested $N = 3$ samples and used the mean response to calculate the effective stiffness.

Actuator characterization

For each part of the actuator characterization, we tested the following number of actuators: force testing $N = 4$, cycling testing $N = 3$, and actuator frequency response $N = 3$. We computed the average response per pressure, cycle, and frequency, respectively. For the force testing and the cycling testing, the averages per pressure are given in tables S3 and S4. We added the SD to the tables because it is representative of the robustness of the actuator response.

User study

The user study was conducted with $N = 32$ participants. For the actuator localization results, we added how many times each participant guessed a certain actuator (correct or incorrect) location given the actual actuation pattern and represent these cumulative results in bar graphs in Fig. 5.

For each stroke duration, we calculated the average continuity and pleasantness ratings across all participants. The SD was added to Fig. 6 to assess the level of consensus in the ratings.

In the confusion matrix shown in Fig. 6C, we display the average scores that participants assigned to each gesture. For instance, if participant 1 assigned 75% attention and 25% happiness to the attention queue and participant 2 assigned 60% attention and 30% love, the attention row of the matrix would show the following average scores: attention, 67.5%; happiness, 12.5%; and love, 15%.

Supplementary Materials

The PDF file includes:

Figs. S1 to S8
Tables S1 to S4
References (*44*–*57*)

Other Supplementary Material for this manuscript includes the following:

Movies S1 and S2
MDAR Reproducibility Checklist

REFERENCES AND NOTES

1. I. Eibl-Eibesfeldt, Human ethology, in *New Aspects of Human Ethology*, A. Schmitt, K. Atzwanger, K. Grammer, K. Schäfer, Eds. (Springer US, 1997), pp. 1–23.
2. M. J. Hertenstein, R. Holmes, M. McCullough, D. Keltner, The communication of emotion via touch. *Emotion* **9**, 566–573 (2009).
3. K. O. Johnson, The roles and functions of cutaneous mechanoreceptors. *Curr. Opin. Neurobiol.* **11**, 455–461 (2001).
4. H. Culbertson, C. M. Nunez, A. Israr, F. Lau, F. Abnousi, A. M. Okamura, A social haptic device to create continuous lateral motion using sequential normal indentation, in *IEEE Haptics Symposium* (IEEE, 2018), pp. 32–39.
5. R. Ackerley, I. Carlsson, H. Wester, H. Olausson, H. B. Wasling, Touch perceptions across skin sites: Differences between sensitivity, direction discrimination and pleasantness. *Front. Behav. Neurosci.* **8**, 54 (2014).
6. M. Y. Tsalamlal, N. Ouarti, J. C. Martin, M. Ammi, Haptic communication of dimensions of emotions using air jet based tactile stimulation. *J. Multimodal User Interfaces* **9**, 69–77 (2015).
7. B. Jumet, Z. A. Zook, A. Yousaf, A. Rajappan, D. Xu, T. F. Yap, N. Fino, Z. Liu, M. K. O'Malley, D. J. Preston, Fluidically programmed wearable haptic textiles. *Device* **1**, 100059 (2023).
8. M. Salvato, S. R. Williams, C. M. Nunez, X. Zhu, A. Israr, F. Lau, K. Klumb, F. Abnousi, A. M. Okamura, H. Culbertson, Data-driven sparse skin stimulation can convey social touch information to humans. *IEEE Trans. Haptics* **15**, 392–404 (2022).
9. K. E. MacLean, Haptic interaction design for everyday interfaces. *Rev. Hum. Factors Ergon.* **4**, 149–194 (2008).
10. C. du Pasquier, T. Chen, S. Tibbits, K. Shea, Design and computational modeling of a 3D printed pneumatic toolkit for soft robotics. *Soft Robot.* **6**, 657–663 (2019).
11. R. F. Shepherd, F. Ilievski, W. Choi, S. A. Morin, A. A. Stokes, A. D. Mazzeo, X. Chen, M. Wang, G. M. Whitesides, Multigait soft robot. *Proc. Natl. Acad. Sci. U.S.A.* **108**, 20400–20403 (2011).
12. S. Biswas, Y. Visell, Emerging material technologies for haptics. *Adv. Mater. Technol.* **4**, 1900042 (2019).
13. W. Wu, H. Culbertson, Wearable haptic pneumatic device for creating the illusion of lateral motion on the arm, in *2019 IEEE World Haptics Conference, WHC 2019* (IEEE, 2019), pp. 193–198.
14. A. Shtarbanov, M. Zhu, N. Colonnese, A. Hajiagha Memar, SleeveIO: Modular and reconfigurable platform for multimodal wearable haptic feedback interactions, in *UIST 2023 - Proceedings of the 36th Annual ACM Symposium on User Interface Software and Technology* [Association for Computing Machinery (ACM), 2023], article no. 70, pp. 1–15.
15. S. Kanjanapas, C. M. Nunez, S. R. Williams, A. M. Okamura, M. Luo, Design and analysis of pneumatic 2-DoF soft haptic devices for shear display. *IEEE Robot. Autom. Lett.* **4**, 1365–1371 (2019).

16. M. Zhu, A. H. Memar, A. Gupta, M. Samad, P. Agarwal, Y. Visell, S. J. Keller, N. Colonnese, PneuSleeve: In-fabric multimodal actuation and sensing in a soft, compact, and expressive haptic sleeve, in *Conference on Human Factors in Computing Systems - Proceedings* (ACM, 2020), pp 1–12.
17. M. Raitor, J. M. Walker, A. M. Okamura, H. Culbertson, WRAP: Wearable, restricted-aperture pneumatics for haptic guidance, in *Proceedings of the IEEE International Conference on Robotics and Automation* (IEEE, 2017), pp. 427–432.
18. D. J. Spencer, *Knitting Technology: A Comprehensive Handbook and Practical Guide* (Technomic Pub., 2001).
19. P. H. Nguyen, W. Zhang, Design and computational modeling of fabric soft pneumatic actuators for wearable assistive devices. *Sci. Rep.* **10**, 9638 (2020).
20. O. Kilic Afsar, A. Shtarbanov, H. Mor, K. Nakagaki, J. Forman, K. Modrei, S. H. Jeong, K. Hjort, K. Höök, H. Ishii, OmniFiber: Integrated fluidic fiber actuators for weaving movement based interactions into the fabric of everyday life, in *UIST 2021 - Proceedings of the 34th Annual ACM Symposium on User Interface Software and Technology* (ACM, 2021), pp. 1010–1026.
21. Y. Luo, K. Wu, T. s. Palacios, W. Matusik, Knitui: Fabricating interactive and sensing textiles with machine knitting, in *Proceedings of the 2021 CHI Conference on Human Factors in Computing Systems* (ACM, 2021), article no. 668, 10.1145/3411764.3445780.
22. Y. Luo, K. Wu, A. Spielberg, M. Foshey, D. Rus, T. Palacios, W. Matusik, Digital fabrication of pneumatic actuators with integrated sensing by machine knitting, in *CHI '22: Proceedings of the 2022 CHI Conference on Human Factors in Computing Systems* (ACM, 2022), article. no. 175, 10.1145/3491102.3517577.
23. J. H. Kim, K. Huang, S. White, M. Conroy, C. H.-L. Kao, KnitDermis: Fabricating tactile on-body interfaces through machine knitting, in *DIS '21: Proceedings of the 2021 ACM Designing Interactive Systems Conference* (ACM, 2021), pp. 1183–1200.
24. J. H. Kim, S. D. Patil, S. Matson, M. Conroy, C. H.-L. Kao, KnitSkin: Machine-knitted scaled skin for locomotion, in *CHI Conference on Human Factors in Computing Systems* (ACM, 2022), pp. 1–15.
25. V. Sanchez, C. J. Payne, D. J. Preston, J. T. Alvarez, J. C. Weaver, A. T. Atalay, M. Boyvat, D. M. Vogt, R. J. Wood, G. M. Whitesides, C. J. Walsh, Smart thermally actuating textiles. *Adv. Mater. Technol.* **5**, 2000383 (2020).
26. J. H. Kim, J. Stilling, M. O'Dell, C. H.-L. Kao, KnitDema: Robotic textile as personalized edema mobilization device, in *Proceedings of the 2023 CHI Conference on Human Factors in Computing Systems* (ACM, 2023), pp. 1–19.
27. E. Churchill, J. T. McConville, *Sampling and Data Gathering Strategies for Future USAF Anthropometry* (Aerospace Medical Research Laboratory, 1976).
28. R. W. Cholewiak, A. A. Collins, Vibrotactile localization on the arm: Effects of place, space, and age. *Percept. Psychophys.* **65**, 1058–1077 (2003).
29. M. F. Nolan, Two-point discrimination assessment in the upper limb in young adult men and women. *Phys. Ther.* **62**, 965–969 (1982).
30. A. Shtarbanov, FlowIO development platform - The pneumatic Raspberry Pi for soft robotics in *Conference on Human Factors in Computing Systems - Proceedings* (ACM, 2021), pp. 1–6.
31. A. Shrivastava, Programmable-Air; https://www.programmableair.com/.
32. S. J. Kim, H. Chang, J. Park, J. Kim, Design of a portable pneumatic power source with high output pressure for wearable robotic applications. *IEEE Robot. Autom. Lett.* **3**, 4351–4358 (2018).
33. A. Schirmer, I. Croy, R. Ackerley, What are C-tactile afferents and how do they relate to "affective touch"? *Neurosci. Biobehav. Rev.* **151**, 105236 (2023).
34. M. J. Hertenstein, D. Keltner, B. App, B. A. Bulleit, A. R. Jaskolka, Touch communicates distinct emotions. *Emotion* **6**, 528–533 (2006).
35. S. C. Hauser, S. McIntyre, A. Israr, H. Olausson, G. J. Gerling, Uncovering human-to-human physical interactions that underlie emotional and affective touch communication, in *2019 IEE World Haptics Conference (WHC)* (IEEE, 2019), pp. 407–412.
36. A. Bhattacharyya, On a measure of divergence between two multinomial populations. *Sankhyā: Indian J. Stat.* **7**, 401–406 (1946).
37. K. Singal, M. S. Dimitriyev, S. E. Gonzalez, A. P. Cachine, S. Quinn, E. A. Matsumoto, Programming mechanics in knitted materials, stitch by stitch. *Nat. Commun.* **15**, 2622 (2024).
38. M. Schünke, E. Schulte, U. Schumacher, *Thieme Atlas of Anatomy: General Anatomy and Musculoskeletal System* (Thieme, 2006).
39. G. Huisman, Social touch technology: A survey of haptic technology for social touch. *IEEE Trans. Haptics* **10**, 391–408 (2017).
40. A. S. MacKlin, J. M. Yau, M. K. O'Malley, Evaluating the effect of stimulus duration on vibrotactile cue localizability with a tactile sleeve. *IEEE Trans. Haptics* **14**, 328–334 (2021).
41. E. Y. Bann, J. J. Bryson, Measuring cultural relativity of emotional valence and arousal using semantic clustering and Twitter, in *Cooperative Minds: Social Interaction and Group Dynamics - Proceedings of the 35th Annual Meeting of the Cognitive Science Society, CogSci 2013*, M. Knauff, Ed. (Cognitive Science Society, 2013), pp. 1809–1814.
42. ASTM Standard D4694-09, 2020, "Standard test method for deflections with a falling-weight-type impulse" (ASTM International, 2020).
43. M. M. Bradley, P. J. Lang, Measuring emotion: The self-assessment manikin and the semantic differential. *J. Behav. Ther. Exp. Psychiatry* **25**, 49–59 (1994).
44. D. Nair, G. Stankaitis, S. Duback, R. Geoffrion, J. B. Jackson, Handwriting correction system using wearable sleeve with optimal tactor configuration, in *2021 18th International Conference on Ubiquitous Robots, UR 2021* (IEEE, 2021), pp. 283–289.
45. Y. Liu, S. Nishikawa, Y. A. Seong, Thermocaress: A wearable haptic device with illusory moving thermal stimulation, in *Proceedings of the 2021 CHI Conference on Human Factors in Computing Systems* (ACM, 2021), article no. 214.
46. E. Leroy, R. Hinchet, H. Shea, Multimode hydraulically amplified electrostatic actuators for wearable haptics. *Adv. Mater.* **32**, 2002564 (2020).
47. E. M. Young, A. H. Memar, P. Agarwal, N. Colonnese, Bellowband: A pneumatic wristband for delivering local pressure and vibration, in *2019 IEEE World Haptics Conference, WHC 2019* (IEEE, 2019), pp. 55–60.
48. S. Basu, J. Tsai, A. Majewicz, Evaluation of tactile guidance cue mappings for emergency percutaneous needle insertion, in *IEEE Haptics Symposium, HAPTICS* (IEEE, 2016), pp. 106–112.
49. G. Huisman, A. Darriba Frederiks, B. Van Dijk, D. Hevlen, B. Krose, The TaSSt: Tactile sleeve for social touch, in *2013 World Haptics Conference, WHC 2013* (IEEE, 2013), pp. 211–216.
50. K. Bark, J. Wheeler, G. Lee, J. Savall, M. Cutkosky, A wearable skin stretch device for haptic feedback, in *Proceedings - 3rd Joint EuroHaptics Conference and Symposium on Haptic Interfaces for Virtual Environment and Teleoperator Systems, World Haptics 2009* (IEEE, 2009), pp. 464–469.
51. H. P. Chien, M. C. Wu, C. C. Hsu, Flowing-haptic sleeve: Research on apparent tactile motion applied to simulating the feeling of flow on the arm, in *UbiComp/ISWC 2021 - Adjunct Proceedings of the 2021 ACM International Joint Conference on Pervasive and Ubiquitous Computing and Proceedings of the 2021 ACM International Symposium on Wearable Computers* (ACM, 2021), pp. 550–554.
52. C. Y. Chen, Y. Y. Chen, Y. J. Chung, N. H. Yu, Motion guidance sleeve: Guiding the forearm rotation through external artificial muscles, in *Conference on Human Factors in Computing Systems - Proceedings* (ACM, 2016), pp. 3272–3276.
53. V. R. Borkowska, A. McConnell, S. Vijayakumar, A. Stokes, A. D. Roche, A haptic sleeve as a method of mechanotactile feedback restoration for myoelectric hand prosthesis users. *Front. Rehabilit. Sci.* **3**, 806479 (2022).
54. J. Weda, D. Kolesnyk, A. Mader, J. van Erp, Experiencing touch by technology, in *Haptics: Science, Technology, Applications: 13th International Conference on Human Haptic Sensing and Touch Enabled Computer Applications, EuroHaptics 2022, Hamburg, Germany, May 22–25, 2022, Proceedings*, H. Seifi, A. M. L. Kappers, O. Schneider, K. Drewing, C. Pacchierotti, A. Abbasimoshaei, G. Huisman, T. A. Kern, Eds. , vol 13235 of *Lecture Notes in Computer Science* (Springer, 2022), pp. 110–118.
55. H. Z. Tan, C. M. Reed, Y. Jiao, Z. D. Perez, E. C. Wilson, J. Jung, J. S. Martinez, F. M. Severgnini, Acquisition of 500 English words through a TActile Phonemic Sleeve (TAPS). *IEEE Trans. Haptics* **13**, 745–760 (2020).
56. Z. Zhang, R. Héron, E. Lecolinet, F. Detienne, S. Safin, Visualtouch: Enhancing affective touch communication with multi-modality stimulation, in *ICMI 2019 - Proceedings of the 2019 International Conference on Multimodal Interaction* (ACM, 2019), pp. 114–123.
57. A. Papadopoulou, J. Berry, T. Knight, R. Picard, Affective sleeve: Wearable materials with haptic action for promoting calmness, in *Distributed, Ambient and Pervasive Interactions: 7th International Conference, DAPI 2019, Held as Part of the 21st HCI International Conference, HCII 2019, Orlando, FL, USA, July 26–31, 2019, Proceedings*, N. Streitz, S. Konomi, Eds., vol. 11587 of *Lecture Notes in Computer Science* (Springer, 2019), pp. 304–319.

Acknowledgments: We thank P. Liu, E. Sigin, and J. Jang for the support in collecting experimental data and T. Buchner for assisting in hardware part sourcing. We also acknowledge the contributions of A. Parker, L. Ambali, and S. Williams for their assistance with physical prototyping, early design ideation, and photographic documentation. **Funding:** This work was supported in part by the National Science Foundation grant nos. 2301355 and 2301356. **Author contributions:** Conceptualization: C.d.P., I.S., and A.O. Methodology: C.d.P., L.Te., I.S., L.Ti., and A.O. Investigation: C.d.P., L.Te., I.S., L.Ti., L.P., and T.C. Visualization: C.d.P. and L.Te. Funding acquisition: C.d.P., T.C., S.T., and A.O. Project administration: C.d.P. Supervision: C.d.P., T.C., S.T., and A.O. Writing—original draft: C.d.P., L.Te., I.S., and L.Ti. Writing—review and editing: C.d.P., S.T., and A.O. **Competing interests:** C.d.P., A.M.O., S.T., L.T., and I.S. are inventors on pending patent 63/612 894 ("Wearable device concept powered by a combination of soft pneumatic actuators and variable stiffness"). The other authors declare that they have no conflicts of interest. **Data and materials availability:** All uniaxial test data are freely available for download using the following link: https://doi.org/10.25740/jk534ft2383.

Submitted 13 February 2024
Accepted 19 November 2024
Published 18 December 2024
10.1126/scirobotics.ado3887